American Mineralogist, Volume 88, pages 159–166, 2003

The effect of ionizing radiation on uranophane

SATOSHI UTSUNOMIYA,[1] LU-MIN WANG,[1] MATT DOUGLAS,[3] SUSAN B. CLARK,[3] AND RODNEY C. EWING[1,2,*]

[1]Department of Nuclear Engineering and Radiological Sciences, University of Michigan, Ann Arbor, Michigan 48109-2104, U.S.A.
[2]Department of Geological Sciences, University of Michigan, Ann Arbor, Michigan 48109-2104, U.S.A.
[3]Department of Chemistry, Washington State University, Pullman, Washington 99164-4630, U.S.A.

ABSTRACT

The susceptibility of uranophane, a uranyl sheet silicate, ideally $Ca(UO_2)_2(SiO_3OH)_2(H_2O)_5$, to ionizing irradiation has been evaluated by systematic irradiations with 200 keV electrons over the temperature range 94 to 573 K. High-resolution transmission electron microscopy revealed that amorphous domains formed locally, concurrently with a gradual disordering of the entire structure. Amorphization doses at room temperature were 1.1×10^{10} Gy for uranophane, 1.3×10^{10} Gy for Sr-substituted uranophane, and 1.9×10^{10} Gy for Eu-substituted uranophane; thus, there was an increase in amorphization dose with increasing average atomic mass. At 573 K, the amorphization dose of uranophane was 2.0×10^{11} Gy. The temperature dependence of the amorphization dose of uranophane has two stages; ≤413 K and >413 K. Based on a defect accumulation model, the effective activation energies for amorphization at each stage are 0.0440 eV and 0.869 eV, respectively. This suggests that the presence of H_2O (and OH^-) reduce the energy deposition required to cause amorphization. Above 413 K, the amorphization dose increased due to the absence of H_2O and OH^- and the absence of radiolytic decomposition of H_2O and OH^-.

INTRODUCTION

Uranophane ($Ca[(UO_2)(SiO_3OH)]_2(H_2O)_5$; $P2_1$; $Z = 2$) is the most common uranyl-silicate, precipitating from near neutral to alkaline ground waters that contain dissolved Si and Ca (Finch and Murakami 1999). Uranophane is a common alteration product in uranium deposits and an expected alteration product of used nuclear fuel in a geologic repository under oxidizing conditions.

The crystal structure of α-uranophane is well known (Smith et al. 1957; Stohl and Smith 1981; Ginderow 1988). Alpha uranophane consists of alternating stacks of U-Si-O sheets with interlayer cations bonded to water molecules or hydroxyl in the **a*** direction (Fig. 1). The two-dimensional anion topology in the U-Si-O sheet is best described as chains of edge-sharing pentagons (P) connected through chains of alternating edge-sharing triangles and squares. The topology can alternatively be described as a chain-stacking sequence consisting of alternating "arrowhead" chains (U, D, and R, following the nomenclature of Miller et al. 1996). Sklodowskite, $Mg[(UO_2)(SiO_3OH)]_2(H_2O)_6$, $C2/m$, has the same anion sheet structure as α-uranophane, but the interlayer cation is Mg instead of Ca. There is a polymorph of uranophane, β-uranophane, that has a different uranyl silicate sheet structure with a different orientation of the SiO_4 tetrahedra that results in a different interlayer configuration (Burns 1999). In this study, only the α-uranophane structure was investigated.

Part of motivation for this study is that spent nuclear fuel and its corrosion products will be subjected to a high radiation field, one that can result in substantial and important property changes. Spent nuclear fuel and its corrosion products will be subjected to a combination of high fluence irradiations from α-, β-particles, γ-rays, and recoil nuclei for at least 10^2–10^3 years. The annual absorbed dose due to β-decay in spent nuclear fuel is 1.8×10^5 Gy/year at 100 years after discharge (Hedin 1997), thus the total absorbed dose can reach 10^7–10^8 Gy. The total absorbed dose in a high level nuclear waste form can be as high as 10^{10} Gy (Weber et al. 1997).

In order to provide for consistency in units, quantities for dose follow the International Commission on Radiological Units and Measurements (ICRU) and the International Commission on Radiological Protection (ICRP). In some cases, radiation quantities are also defined based on previous work (Shani 1991; Knoll 2000; Tsoulfanidis 1983). Because only a monodirectional beam was used in our experiments, flux (or electron flux) is defined as the number of electrons per unit area, per unit time and fluence (electron fluence), F, is the time integral of the flux over the exposure duration. Dose (or absorbed dose), D, is defined as the energy absorbed per unit mass of material, and dose rate (or absorbed dose rate) is the quotient of incremental absorbed dose by the absorption time. In a previous study of electron irradiation of zeolite, Wang et al. (2000) used dose, D, interchangeably with fluence, F. Although this is a common usage in previous studies, this has lead to confusion.

The high rate of energy absorption through ionization and electronic excitation from α- and β-decay can also cause significant self-heating; the temperature increase depends on the

* E-mail: rodewing@umich.edu

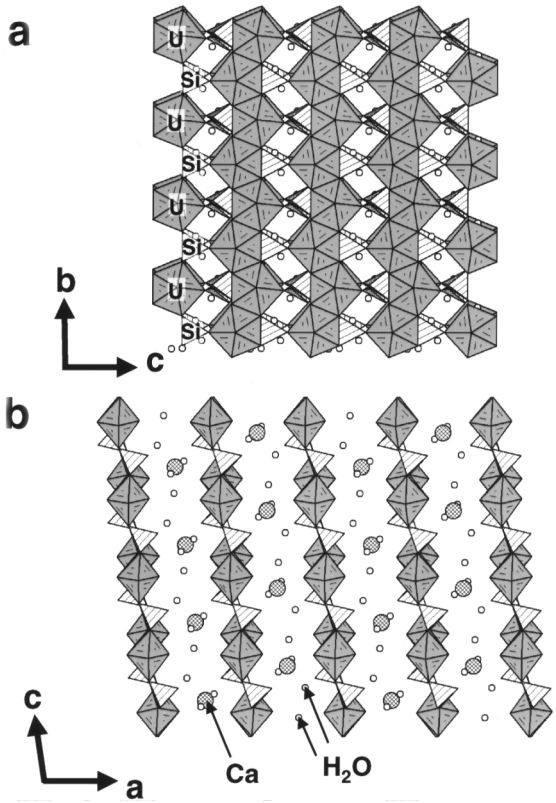

FIGURE 1. The structure of uranophane viewed along (**a**) [100] and (**b**) [010]. Ca and H_2O exist in the interlayer of the sheet structure after Burns (1999)

thermal loading of the geologic repository. At the proposed repository at Yucca Mountain, temperatures as high as 573 K may occur initially and remain above 373–423 K for several hundred years after emplacement (Weber et al. 1997). Therefore the temperature dependence of the radiation damage effects is critical to understanding the radiation response of alteration products that form at the surface of the used nuclear fuel.

The secondary alteration products of spent nuclear fuel in an oxidizing environment will be a variety of uranyl oxy-hydroxides, silicates and phosphates, depending on the groundwater composition (Finch and Ewing 1992). Recently there has been much interest in these secondary uranyl phases, as they may become "sinks" for important radionuclides, such as ^{237}Np (Burns et al. 1997). Uranophane has been identified in corrosion tests of used nuclear fuels (Buck et al. 1998; Finch et al. 1999), and it is a common alteration product of uranium-phases in an oxidizing environment.

PREVIOUS WORK

There have been few systematic studies of radiation-induced amorphization due to ionizing radiation of minerals and ceramics (Hobbs et al. 1994). A theoretical model of amorphization under electron irradiation has been developed by Motta and Olander (1990) based on data for metals and intermetallics. In their model, amorphization occurs when the target has been provided with an additional amount of energy that is greater than the free energy difference between crystalline and amorphous states. The total free energy is the sum of the free energy increase due to the point defect concentration and the increase due to chemical disordering. The model is based on radiation effects in metals and is certainly less applicable to more complex, ceramic materials (Hobbs et al. 1994).

Hobbs and Pascucci (1980) have suggested a mechanism for the ionization-induced amorphization in SiO_2. They propose two stages in the amorphization process: (1) heterogeneous nucleation and growth of disordered strain centers involving migration of point defects, and (2) a gradual homogenous disordering in the remaining matrix. The mechanism is based on a model of radiolysis: (1) instability of Si-O bonds due to electronic excitation and the breaking of bonds; and (2) the formation of a peroxy linkage at other oxygen sites and the creation of oxygen vacancies. The highly localized oxygen vacancies can cause Si-O tetrahedra reorientation. Hobbs and Pascucci (1980) also suggested that water in the form of hydrolyzed bonds may serve as nucleation centers of defects.

Many ion-irradiation experiments of ceramics and minerals have been completed as part of systematic investigations of radiation-induced amorphization (Ewing et al. 2000). Irradiation by electrons is, however, an entirely different process from these heavy ion irradiations that directly produce displacement cascades in the target (Wang and Ewing 1992). The more relevant studies are electron and proton irradiations of hydrated phases, such as zeolite (Yokota et al. 1984; Wang et al. 2000; Mitome et al. 2001; Gu et al. 2000). In the case of hydrated ceramics, such as clays and zeolites, the solid-state radiolysis of molecular water plays an important role in the decomposition process (Wang et al. 2000). The formation of radicals, such as $(OH)^-$ and $(H_2O)_n^-$, can induce the collapse of the structure. As an example, light cations can be displaced by direct ionization or the formation of $(OH)^-$ radicals. The "water radical model" is supported by evidence for bubble formation in zeolite due to the slow release rate of water (Wang et al. 2000). Mitome et al. (2001) have proposed a model of electron irradiation-induced amorphization in zeolite based on competition between defect creation and annihilation. This model has been successfully applied to interpret the temperature dependence of amorphi-zation dose in zeolite (Mitome et al. 2001).

The purposes of this study are: (1) to investigate and model the effects of ionizing radiation on uranophane and related structures; (2) to measure the critical amorphization dose as a function of temperature.

EXPERIMENTAL METHODS

The samples for the irradiation experiments were synthetic uranophane, sklodowskite $[Mg(UO_2)_2(SiO_3OH)_25H_2O$; $C2/m$; $Z = 2]$, and uranophane in which 100% of the Ca has been replaced by Sr and Eu. These samples are referred to as U-Ca, U-Mg, U-Sr, and U-Eu, respectively. The procedure for the synthesis was the same as that described by Nguyen et al. (1992). The products of the synthesis were characterized by powder X-ray diffraction analysis (XRD). All electron irradiation experiments were conducted in a JEOL JEM-2010F transmission electron microscope (TEM) operated at 200 keV. The

samples were irradiated in the temperature range 94 to 573 K using a GATAN Smart Controller as a heating and cold stage. The sample holder was tilted 20° from the major zone axis to minimize electron channeling. The electron flux varied from 7.01×10^{17} to 6.11×10^{18} $e^-/cm^2/s$. The crystalline-to-amorphous transition was monitored in situ by selected area electron diffraction (SAED) patterns (Fig. 2). The change in intensity of the diffraction maxima in the SAED was observed with a charge-coupled device (CCD) camera. The intensity of diffraction maxima was determined by counting the number of electrons. By this procedure, a square region of interest was established around the diffraction maximum of interest (Fig. 3a). Then a histogram for the number of pixels that have the same number of electron counts was produced by running the option "analysis" in Digital Micrograph (Gatan Inc.). The background electron count was based on the average value of the peak with lower counts, and the diffraction maximum is the largest count of electrons (Fig. 3b). Because the background counts can increase due to the appearance of a diffraction halo caused by the formation of amorphous material, the actual intensity measured is the maximum value after background subtraction. High-resolution electron microscopy (HRTEM) was completed at the same time.

RESULTS

SAED patterns along the [100] zone show a gradual decrease of intensity for all diffraction maxima with increasing electron fluence at 278 K (Fig. 2). Some diffraction spots, for which the intensity was measured by a CCD camera, are indexed in Figure 3a. A typical histogram for the diffraction spot 020 is shown in Figure 3b. The horizontal axis gives the number of electrons in the pixel, and the vertical axis represents the number of pixels having the same number of electron counts.

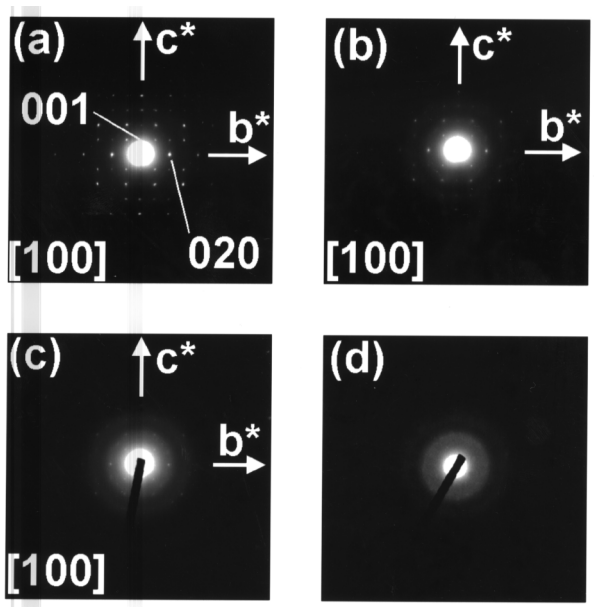

FIGURE 2. SAED of the radiation-induced transition for uranophane irradiated at room temperature. (**a**) un-irradiated, (**b**) 3.2, (**c**) 6.3, and (**d**) 7.9 ($\times 10^{19}$ e^-/cm^2).

The results of the detailed measurement of the intensity change are shown in Figure 3c. The change in the maximum electron count after background subtraction revealed that the intensity

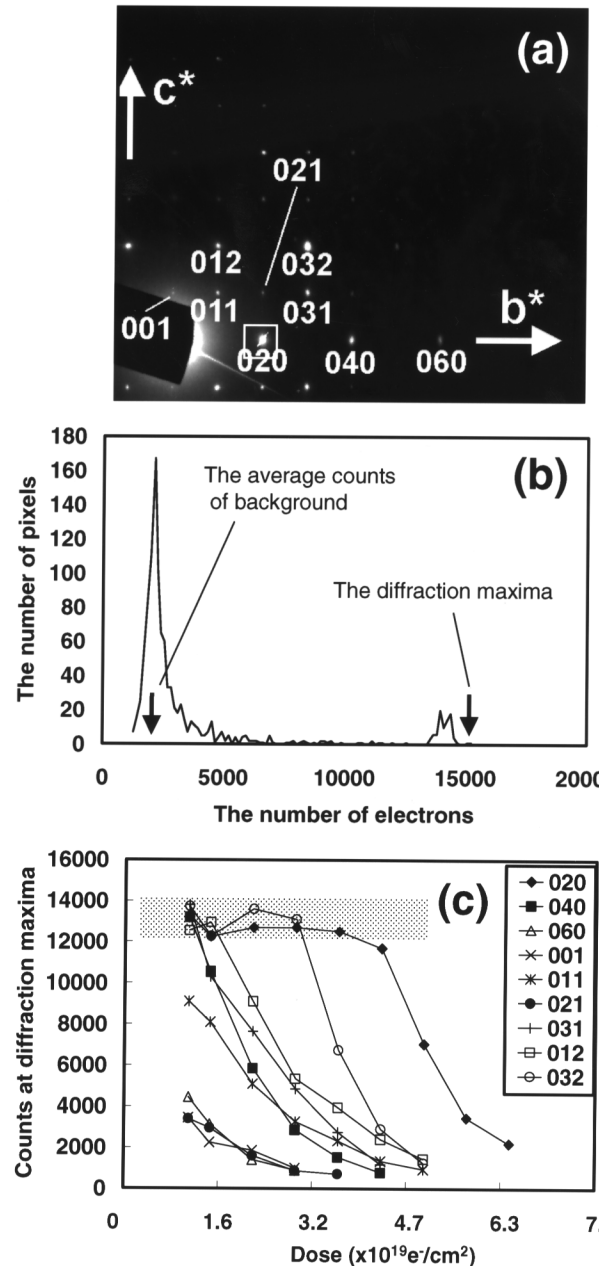

FIGURE 3. (**a**) SAED of uranophane at initial stage, in which the diffraction maxima of the indexed spots were counted by a charge-couple device (CCD) camera. The white squares around the diffraction maxima represent regions of interest used to produce the histogram. (**b**) The intensity was counted as the number of electrons. The real number of electrons in the diffraction maxima was the measured value less the average number of background electrons. (**c**) Change in the intensity of selected diffraction spots shows an exponential decrease with increasing fluence. The upper gray band represents the maximum possible counts for the CCD camera. Thus, the data points within the band are not reliable.

of all indexed spots decreased exponentially (that is, $I = Ae^{-BD_a}$: where A and B are arbitrary coefficients). The crystalline-to-amorphous transition required a lower fluence as the amorphous regions became larger, supporting a nucleation and growth mechanism. The same phenomena has been observed in electron-irradiated zeolite (Mitome et al. 2001)

HRTEM images of the crystalline-to-amorphous transition show the gradual disruption of the periodic structure (Fig. 4). The disordering process occurs uniformly, but isolated amorphized regions appeared prior to complete amorphization (within the circles in Figs. 4a and b). Bubble formation due to released oxygen or hydrogen was not observed during irradiation, as is frequently the case for electron-irradiated zeolite (Wang et al. 2000). Table 1 summarizes the amorphization fluence, F_c, and the absorbed electronic dose, D_c, for uranophane from 94 to 573 K.

The temperature dependence of the amorphization fluence, F_c, for Ca-uranophane is shown in Figure 5. There are two stages in the F_c-T curve: F_c increases gradually up to 413 K and then increases rapidly above 413 K. Prior to irradiation at high temperatures, the SAED patterns along [100] were observed in order to determine whether there was a thermal effect at 573 K. No change was evident in the SAED pattern; thus, at least in that part of the structure viewed perpendicular to **a***, that is the **b**-**c** plane, there was no evidence for thermal breakdown of the uranophane structure. However, it is likely that H_2O molecules are driven from the interlayer sites between the **b**-**c** planes at temperatures above 413 K.

The average amorphization fluence and dose for the uranyl-silicates with other cations substituted for Ca are plotted vs. the atomic mass of the substituting cations in Figure 6. The uranyl-silicates that retain the uranophane structure (open circles) show a trend in which F_c increases with increasing atomic mass of the substituting cation. The absorbed electronic dose, D_c, also reveals the same trend. A similar relationship between amorphization dose and the mass of the target has been observed in other ion irradiation experiments (Meldrum et al. 1997; Utsunomiya et al. 2002). The F_c of sklodowskite (U-Mg) is 9.6×10^{19} (e^-/cm^2); thus, the critical amorphization fluence is similar to that of the uranophane samples.

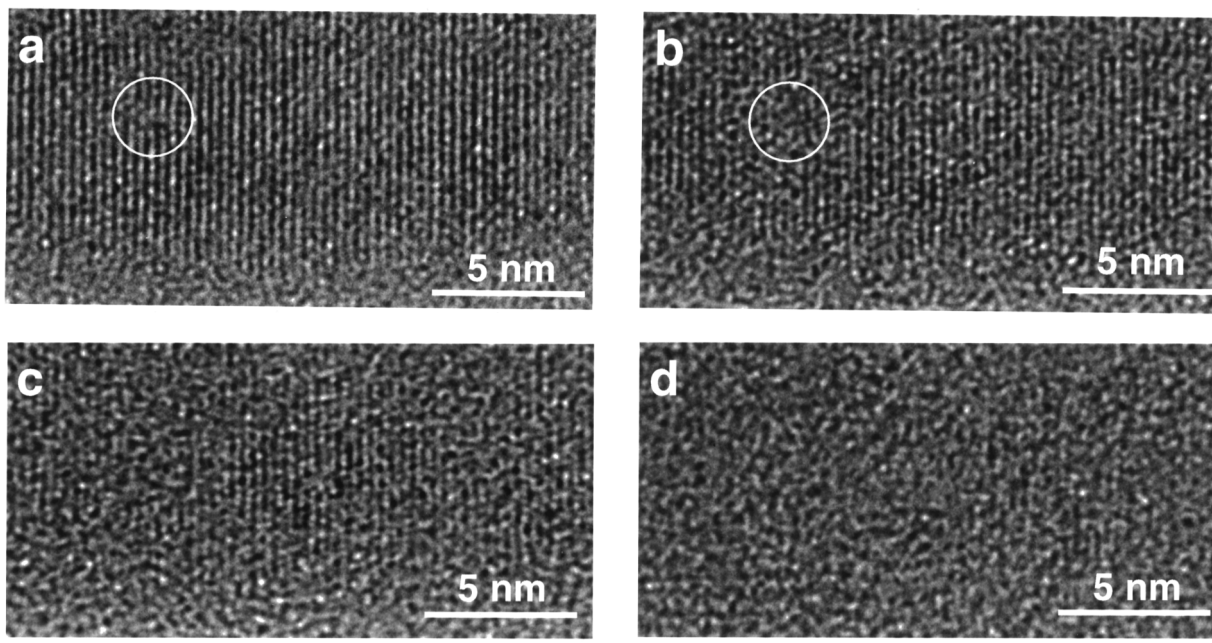

FIGURE 4. The HRTEM of transition for the uranophane irradiated at the room temperature. (**a**) 1.6, (**b**) 3.2, (**c**) 4.7, and (**d**) 7.9 ($\times 10^{19}$ e^-/cm^2).

TABLE 1. The amorphization fluence, F_c (x10^{19} e^-/cm^2) and the absorbed electronic dose, D_c (x10^{10} Gy), of uranophane at various temperatures

T (K)	94	143	193	243	298	353	413	453	503	523	573
F_c	3.95	5.06	6.23	6.29	9.20	8.56	11.1	20.4	113	236	1337
	3.66	5.98	5.68	6.12	8.48	8.17	10.3	21.9	136		1421
	4.15	4.96	5.44	6.67	7.32	9.20	9.57	20.6	133		
	3.94	5.96	6.06	7.15	8.61	7.67	11.4	20.9			
	4.66	5.15	6.01	6.51	6.82	8.58	10.2	21.7			
	4.03	5.20	5.47	7.21	6.81	8.98					
	4.72	5.24	6.07	6.85	7.67	8.22					
	3.86	5.32	5.68	5.89	8.41	9.68					
	4.32	4.57	5.60	6.57	7.87	7.64					
	4.55	4.85	5.70	7.01							
Average F_c	4.18	5.23	5.79	6.63	7.91	8.52	10.5	21.1	127	236	1379
D_c	0.602	0.753	0.833	0.954	1.14	1.23	1.51	3.04	18.3	34.0	198

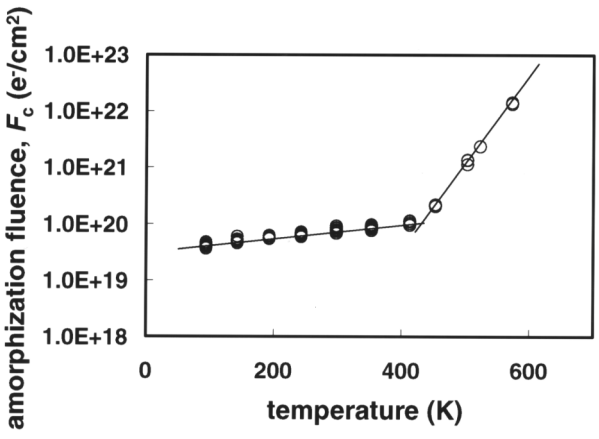

FIGURE 5. The temperature dependence of the amorphization fluence, F_c, for the electron-irradiated uranophane.

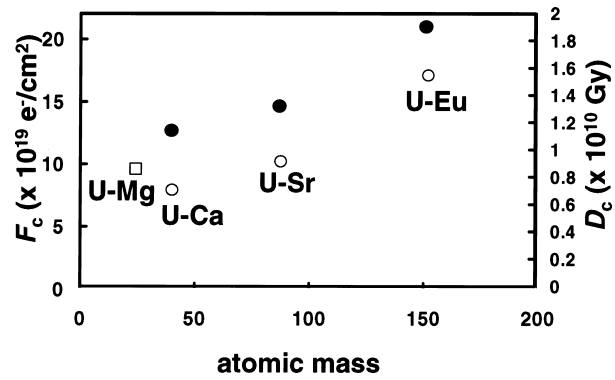

FIGURE 6. The amorphization fluence, F_c, and the absorbed electronic dose, D_c, for other uranyl silicates. Plotted as a function of the increasing atomic mass of the cations substituting for Ca. U-Ca, U-Sr, and U-Eu have the uranophane structure (open circles). U-Mg is sklodowskite. Closed circles represent the electronic dose, D_c, in Gy.

DISCUSSION

Energy deposition from electron irradiation of a sample can be estimated from the stopping power of the target composition. The total stopping power is the sum of the ionization, elastic scattering, and radiative contributions. The radiative stopping power is due to the energy depletion by electromagnetic radiation. The total stopping power is expressed as:

$$\left(-\frac{\mathrm{d}E}{\mathrm{d}x}\right)_{\mathrm{tot}} = \left(-\frac{\mathrm{d}E}{\mathrm{d}x}\right)_{\mathrm{ion}} + \left(-\frac{\mathrm{d}E}{\mathrm{d}x}\right)_{\mathrm{rad}} + \left(-\frac{\mathrm{d}E}{\mathrm{d}x}\right)_{\mathrm{els}} \quad (1)$$

The elastic scattering factor is not significant, as will be described later; thus, the total electronic stopping power is essentially the sum of the first and the second terms. The ionizing stopping power from the volume around an electron track can be calculated based on the stopping-power theory of Bethe using the formulation of Turner (1995). The stopping-power of electrons in MeV/cm is

$$\left(-\frac{\mathrm{d}E}{\mathrm{d}x}\right)_{\mathrm{ion}} = \frac{4\pi k_0^2 e^4 n}{mc^2\beta^2}\left[\ln\frac{mc^2\tau\sqrt{\tau+2}}{\sqrt{2}I} + F(\beta)\right] \times \frac{1}{1.60\times10^{-13}} \times \frac{1}{100} \quad (2)$$

where

$$F(\beta) = \frac{1-\beta^2}{2}\left[1 + \frac{\tau^2}{8} - (2\tau+1)\ln 2\right] \quad (3)$$

$\tau = E_{\mathrm{kin}}/mc^2$, in which E_{kin} is the kinetic energy, τ is the multiple of the electron rest energy mc^2, $k_0 = 1/4\pi\varepsilon_0$, in which ε_0 is the permittivity constant, e is the magnitude of the electron charge, n is the number of electrons per unit volume in the medium, m is the electron rest mass, c is the speed of light in vacuum, β is the ratio of the speed of the particle to the light (V/c), and I is the mean excitation energy of the medium, which is expressed by the following empirical formulae

$$I \cong \begin{cases} 19.0\ \mathrm{eV},\ Z = 1\ (\mathrm{hydrogen}) \\ 11.2 + 11.7\ Z\ \mathrm{eV},\ 2 \le Z \le 13 \\ 52.8 + 8.71\ Z\ \mathrm{eV},\ Z > 13 \end{cases} \quad (4)$$

where Z is the atomic number of the target. For a complex composition, I can be calculated by summing the contributions from the individual constituent elements

$$n \ln I = \sum_i N_i Z_i \ln I_i \quad (5)$$

N_i is atomic density (atoms/cm³) for an element with atomic number Z_i and its mean excitation energy I_i. The I of uranophane (U-Ca) is calculated to be 307.9 eV. The ionizing stopping power of 200 keV electrons in uranophane (U-Ca) is calculated to be 3.40 MeV/cm. For the other uranophane composition in which 100 percent of the Ca was replaced by Eu (U-Eu) and Sr (U-Sr), the mean excitation energies were estimated to be 682.7 and 423.1 eV, respectively. Thus, the ionizing stopping powers for U-Eu and U-Sr are 2.63 and 3.06 MeV/cm, respectively.

The radiative stopping power is negligible in cases where the target material consists of light elements. However, when the target material has elements heavier than lead or the incident electron energy is higher than 1 MeV, the effects of the radiative stopping power must be considered. The radiative stopping power is caused by Bremsstrahlung. An empirical formula gives an approximate value for the radiative stopping power (Turner 1995)

$$\frac{\left(-\frac{\mathrm{d}E}{\mathrm{d}x}\right)_{\mathrm{rad}}}{\left(-\frac{\mathrm{d}E}{\mathrm{d}x}\right)_{\mathrm{ion}}} \cong \frac{ZE}{800} \quad (6)$$

where E is the total energy of electron, $E = E_{\mathrm{kin}} + mc^2$ in MeV. Based on the mole fraction of Z, the radiative stopping power in uranophane (U-Ca) is calculated to be 0.0360 MeV/cm. Thus the contribution of the radiative stopping power is less than 2% as compared with the ionizing stopping power. Finally, the total electronic stopping power is 3.44 MeV/cm and those of the other uranophane compositions, U-Eu and U-Sr, are 2.66 and 3.09 (MeV/cm), respectively.

The total electronic energy deposition, which is same as the absorbed electronic dose, D_c, in Gy = J/kg, can be reduced to the equation:

$$D_c = \left(-\frac{dE}{dx}\right) \times 10^6 \times F_c \times 1.6022 \times 10^{-19} / 3.83 \times 1000 \quad (7)$$

The amorphization dose of the uranophane (U-Ca) at 298 K is 1.14×10^{10} Gy; 1.90×10^{10} Gy for U-Eu; 1.32×10^{10} Gy for U-Sr.

The cross-section for atomic displacement through electron-nucleus collision, σ_d, may be estimated by the expression given by McKinley and Feshbach (1948):

$$\sigma_d = \pi\left(\frac{Ze^2}{mc^2}\right)^2\left(\frac{1}{\beta^4\gamma^2}\right)\left[\left(\frac{E_m}{E_d}-1\right)-\beta^2\ln\frac{E_m}{E_d}+\pi\alpha\beta\left\{2\left[\left(\frac{E_m}{E_d}\right)^{0.5}-1\right]-\ln\frac{E_m}{E_d}\right\}\right] \quad (8)$$

where,

$$\gamma = (1-\beta^2)^{-0.5} \quad (9)$$

$$\alpha \equiv Z\left(\frac{e^2}{\hbar c}\right) \cong \frac{Z}{137} \quad (10)$$

E_d represents the threshold displacement energy. E_m is the maximum transferable energy by collision events:

$$E_m = 2\frac{m}{M}\frac{\left(E_{kin}+2mc^2\right)E_{kin}}{mc^2} \quad (11)$$

in which M is the mass of a nucleus. Under the present experimental conditions, 200 keV, the E_m values for U, Si, Ca, O, and H are calculated to be 2.20, 18.7, 13.1, 32.8, and 521 (eV), respectively. Assuming that E_d of U, Si, Ca, O, and H are 40 (Zinkle and Kinoshita 1997), 23 (Weber et al. 1998), 25 (Ziegler et al. 1985), 28 (Zinkle and Kinoshita 1997), and 10 (Ziegler et al. 1985) (eV), the cross-section, σ_d, of H, O, Ca, and Si were estimated to be 4.26, 2.75, 2.41, and ~0 ($\times 10^{-24}$ cm^2). The value of σ_d for U cannot be estimated by this expression because it is not valid for the high Z elements. However the estimated σ_d in the present study has a tendency such that the higher Z elements have smaller σ_d; thus the σ_d of U can be inferred to be ~ 0 (cm^2). The average displacement cross-section for uranophane is 1.5×10^{-24} (cm^2) per mole fraction. The cross-section can be converted to displacements per atom, dpa, by the following expression when the sample is a thin film and the energy loss is very small (Wang et al. 2000; Nastasi et al. 1996)

$$\text{dpa} = F \cdot \sigma_d \quad (12)$$

in which F is electron fluence (electrons/cm^2). Based on this relation, the displacement damage level at the amorphization dose of uranophane at room temperature is only 0.00012 dpa. Therefore, the number of displacements due to ballistic interactions between electrons and nuclei is too low to cause radiation-induced amorphization of the structure. Although there must be multiple displacements caused by H primary knock-on atoms (PKAs) due to the relatively large E_m (521 eV) of H, these displacements are fewer than the primary displacement events. Assuming that the H atom experiences the maximum in transferable energy, 521 eV, the displacement/ion/Å can be calculated to be 0.0035 using SRIM-2000 (Ziegler et al. 1985), which corresponds to 0.53 displacement/H within the range ~150 A. For about 32 mol% H in uranophane, the dpa by electrons is 0.000038. Thus the displacement by the PKAs is 0.00002 and total maximum dpa is 0.00014. Such a low dpa means that the amorphization of uranophane must be the result of ionization effects and not be due to electron-nuclei collisions.

In materials sensitive to thermal effects or metastable phase formation, the thermal effect is significant in the amorphization process. A previous electron irradiation study in coesite suggested that the critical amorphization dose decreased rapidly at low temperatures (Gong et al. 1996). Studies of zeolite have also revealed abrupt decreases in amorphization dose at low temperatures (Wang et al. 2000). In these cases, thermally induced amorphization processes are dominant. In contrast, thermally induced amorphization is not a major process of the amorphization of uranophane within the temperature range of the present experiments (Fig. 5). Thus, the thermally activated amorphization is not considered in the following discussion.

According to the model by Mitome et al. (2001), defects can recombine and disappear due to radiation-enhanced diffusion. Thus, the increase in the amount of interstitial atoms during a time, dt, is expressed as the sum of an increasing rate of the defect formation by electron irradiation and a decreasing rate due to annihilation:

$$dC = (C_0 - C)j\sigma_{def}\,dt - C^2\sigma_{def}'v_d dt \quad (13)$$

where C, C_0, j, σ_{def} and σ_{def}' are the concentration of defect pairs, the concentration of the initial sites that are orgins of the localized defects, the electron current density, the cross-sections for creation and annihilation of the defects, respectively. Thus, σ_{def} and σ_{def}' are different from σ_d which represents the displacement cross-section. The concentration, C, saturates within a short period, and this is given as:

$$C = \sqrt{\frac{C_0 j\sigma_{def}}{v_d\sigma_{def}'}} \quad (14)$$

in which the defect diffusion rate, v_d, is dependent on the temperature as given by the equation:

$$v_d = v_0 \exp\left(-\frac{E_{dif}}{kT}\right) \quad (15)$$

where E_{dif} and k are the diffusion energy and Boltzmann's constant. Combining Equations 14 and 15

$$C = \sqrt{\frac{C_0 j\sigma_d}{v_d\sigma_d'}}\exp\left(\frac{E_{dif}}{2kT}\right) \quad (16)$$

The probability for breaking down the structure, P, may be expressed by the activation energy to decompose the structure, E_b

$$P \propto C\exp\left(-\frac{E_b}{kT}\right) = \sqrt{\frac{C_0 j\sigma_{def}}{v_d\sigma_{def}'}}\exp\left(-\frac{E_b - E_{dif}/2}{kT}\right) \quad (17)$$

Because C_0, j, σ_{def}, V_d, and σ_{def}' are independent of temperature, the effective activation energy, E_{eff}, is $E_{eff} = E_b - E_{dif}/2$.

The temperature dependence of the critical amorphization fluence, F_c, may be related to the probability of structural destruction described by Equation 17. The correlation may be described as

$$F_c = F_0 + k_r P \quad (18)$$

where F_0 is the amorphization fluence at 0 K and k_r is a correlation coefficient between the F_c and P. Then the F_c-T relationship in Figure 5 can be fitted to two separate stages:

$$F_c = 4.06\times10^{19} + 1.32\times10^{20}\exp\left(-\frac{1.64\times10^4}{kT}\right) \text{ for } T \le 413 \text{ K} \quad (19)$$

$$F_c = 1.06\times10^{20} + 1.09\times10^{30}\exp\left(-\frac{4.49\times10^5}{kT}\right) \text{ for } T > 413 \text{ K} \quad (20)$$

The second stage has a larger activation energy (E_{eff} = 4.49 × 10^5 eV/K) than the first stage (E_{eff} = 1.64 × 10^4 eV/K). The diffusion energy, E_d, does not vary in the same material; thus, the main difference in E_{eff} is attributed to the decomposition energy of the target, E_b. For uranophane, the only difference in the irradiated uranophane above and below 413 K is probably the presence or absence of H_2O and OH^- in the structure. H_2O and OH^- that occur in the interlayer of the sheet structure (Fig. 1b) may dissociate from the structure at ~413 K. In clay minerals, water molecules in the interlayer dehydrate between 373–573 K depending upon the coordination with interlayer cations. For example, dehydration in vermiculite occurs at 423 K (Graf v. Reichenbach and Beyer 1997) and in montmorillonite at 403 K (Mozas et al. 1980). The second stage (> 413 K) in the F_c-T curve corresponds to amorphization of uranophane that does not contain H_2O or OH^-. Mitome et al. (2001) have suggested that the decomposition energy, E_b, of the water-free material is higher than the equivalent structure that contains water; that is, water molecule radicals cause the structure to collapse because of altered charge balance distributions. An alternative explanation for the effect of OH^- is that the OH^- ion can form point-defect complexes and promote radiation damage during electron irradiation. This has been observed in MgO (Kinoshita et al. 1998), and water in the form of hydrolyzed bonds can also be a nucleating agent for point defects (Hobbs and Pascucci 1980). These models suggest that the point defects can form in larger numbers due to the existence of OH^- and H_2O. Thus, radiation-induced amorphization can be accelerated in structures that contain OH^- and H_2O. However, considering that bubble formation has been observed in electron-irradiated zeolite (Wang et al. 2000), the water molecule radicals may be a more important factor in the decomposition energy than the role of OH^- in accelerating the formation of point defects.

The temperature effect of self-heating from β-decay of fission products can drive the temperature as high as 523 K depending on the thermal loading of the disposal strategy for spent nuclear fuel in a geologic repository, and the temperature will decrease to less than 373 K during the first several hundred years of storage. The annual dose due to β-decay is 10^7–10^8 Gy for commercial HLW forms during first several hundred years after discharge from the reactor (Weber et al. 1997), and at a position one meter from the spent nuclear fuel, the annual dose from γ-radiation is 1.8×10^5 Gy/year after 100 years and 8.8×10^2 Gy/year after 200 years (Hedin 1997). Compared to these annual doses, the amorphization dose of uranophane is very high: 10^{10}~10^{11} Gy from room temperature up to 573 K. In addition, the dose rates used in the present experiments were 10^{15}–10^{16} Gy/year, which is 10^7 to 10^{10} higher than the annual dose in the spent nuclear fuel. Thus, these results suggest that the uranyl silicate alteration phases will remain crystalline despite the highly intense γ-field that emanates from the spent nuclear fuel.

ACKNOWLEDGMENTS

The electron irradiation and TEM analysis were conducted at the Electron Micro-beam Analysis Laboratory at the University of Michigan. The authors are grateful for the thoughtful comments on this paper by W.J. Weber, P.C. Burns, and an anonymous reviewer. This work was supported by US-DOE, Office of Basic Energy Sciences under grant DF-FGO3-01ER15138 and the Environmental Management Science Program DE-FG07-97ER14816.

REFERENCES CITED

Buck, E.C., Finch, R.J., Finn, P.A., and Bates, J.K. (1998) Retention of neptunium in uranyl alteration phases formed during spent fuel corrosion. Material Research Society Symposium Proceedings, 506, 87–94.

Burns, P.C. (1999) The crystal chemistry of uranium. In P.C. Burns and R. Finch, Eds., Uranium: Mineralogy, Geochemistry and the Environment, 38, 23–90. Reviews in Mineralogy, Mineralogical Society of America, Washington, D.C.

Burns, P.C., Ewing, R.C., and Miller, M.L. (1997) Incorporation mechanisms of actinide elements into the structures of U^{6+} phases formed during the oxidation of spent nuclear fuel. Journal of Nuclear Materials, 245, 1–9.

Ewing, R.C., Meldrum, A., Wang, L.M., and Wang, S.X. (2000) Radiation-induced amorphization" S.A.T. Redfern and M.A. Carpenter, Eds., 39, 317–361. Reviews in Mineralogy, Mineralogical Society of America, Washington, D.C.

Finch, R. and Ewing, R.C. (1992) The corrosion of uraninite under oxidizing conditions. Journal of Nuclear Materials, 190, 133–156.

Finch, R.J. and Murakami, T. (1999) Systematics and paragenesis of uranium minerals. 38, 91–179. Reviews in Mineralogy, Mineralogical Society of America, Washington, D.C.

Finch, R.J., Buck, E.C., Finn, P.A., and Bates, J.K. (1999) Oxidative corrosion of spent UO_2 fuel in vapor and dripping groundwater at 90 °C. Material Research Society Symposium Proceedings, 556, 431–438.

Gong, W.L., Wang, L.M., Ewing, R.C., and Zhang, J. (1996) Electron-irradiation- and ion-beam-induced amorphization of coesite. Physical Review B, 54, 3800–3808.

Graf v. Reichenbach, H. and Beyer, J. (1997) Dehydration and rehydration of vermiculites: III. Phlogopitic Sr- and Ba-vermiculite. Clay Minerals, 32, 573–586.

Ginderow, P.D. (1988) Structure de l'Uranophane α, $Ca(UO_2)_2(SiO_3OH)_25H_2O$. Acta Crystallographica, C44, 421–424.

Gu, B.X., Wang, L.M., and Ewing, R.C. (2000) The effect of amorphization on the Cs ion exchange and retention capacity of zeolite-NaY. Journal of Nuclear Materials, 278, 64–72.

Hedin, A. (1997) Spent nuclear fuel – How dangerous is it? A report from the project "Description of risk", Technical report 97–13, Swedish Nuclear Fuel and Waste Management Co, Stockholm, Sweden, p 60.

Hobbs, L.W. and Pascucci, M.R. (1980) Radiolysis and defect structure in electron-irradiated α-quartz. Journal de Physique, 7, C6.237–C6.242.

Hobbs, L.W., Clinard, F.W. Jr., Zinkle, S.J., and Ewing, R.C. (1994) Radiation effects in ceramics. Journal of Nuclear Materials, 216, 291–321.

Kinoshita, C., Sonoda, T., and Manabe, A. (1998) Influence of OH^- ion point-defect complexes on the electron irradiation damage response of MgO crystals. Philosopical Magazine A, 78, 657–670.

Knoll, G.F. (2000) Radiation Detection and Measurement, 3rd edition. Wiley, New York.

McKinley, W.A. and Feshbach, H. (1948) The coulomb scattering of relativistic electrons by nuclei. Physical Review, 74, 1759–1763.

Meldrum, A., Boatner, L.A., and Ewing, R.C. (1997) Displacive radiation effects in the monazite- and zircon- structure orthosilicates. Physical Review B, 56, 13805–13814.

Miller, M.L., Finch, R.J., Burns, P.C., and Ewing, R.C. (1996) Description and classification of uranium oxide hydrate sheet topologies. Material Research Society Symposium Proceedings, 412, 369–376.

Mitome, M., Bando, Y., Kurashima, K., and Kitami, Y. (2001) Temperature dependency of radiation damage in inorganic materials by 300 keV electrons. Journal of Electron Microscopy, 50, 245–249.

Motta, A.T. and Olander, D.R. (1990) Theory of electron-irradiation-induced

amorphization. Acta Metallurgica, 38, 2175–2185.
Mozas, T., Bruque, S., and Rodriguez, A. (1980) Effect of thermal treatment on lanthanide montmorillonites: Dehydration. Clay Minerals, 15, 421–428.
Nastasi, M., Mayer, J.W., and Hirvonen, J.K. (1996) Ion-solid interactions: Fundamentals and applications, p. 160. Cambridge University, Cambridge, U.K.
Nguyen, S.N., Silva, R.J., Weed, H.C., and Andrews, J.E. Jr. (1992) Standard Gibbs free energies of formation at the temperature 303.15 K of four uranyl silicates: soddyite, uranophane, sodium boltwoodite, and sodium weeksite. Journal of Chemical Thermodynamics, 24, 359–376.
Shani, G. (1991) Radiation dosimetry instrumentation and methods. CRC Press, Florida.
Smith, D.K. Jr., Gruner, J.W., and Lipscomb, W.N. (1957) The crystal structure of uranophane, $Ca(H_3O)_2(UO_2)_2(SiO_4)_2(H_2O)_3$. American Mineralogist, 42, 594–618.
Stohl, F.V. and Smith, D.K. (1981) The crystal chemistry of the uranyl silicate minerals. American Mineralogist, 66, 610–625.
Tsoulfanidis, N. (1983) Measurement and detection of radiation. McGraw-Hill, New York.
Turner, J.E. (1995) Atoms, radiation, and radiation protection. Wiley, New York.
Utsunomiya, S., Wang, L.M., Yudintsev, S., and Ewing, R.C. (2002) Ion irradiation-induced amophization and nano-crystal formation in garnets, Journal of Nuclear Materials, 303, 177–187.
Wang, L.M. and Ewing, R.C. (1992) Ion-beam-induced amorphization of complex ceramic materials—minerals. Materials Research Society Bulletin, 17, 38–44.
Wang, S.X., Wang, L.M., and Ewing, R.C. (2000) Electron and ion irradiation of zeolites. Journal of Nuclear Materials, 278, 233–241.
Weber, W.J., Ewing, R.C., Angell, C.A., Arnold, G.W., Cormack, A.N., Delaye, J.M., Griscom, D.L., Hobbs, L.W., Navrotsky, A., Price, D.L., Stoneham, A.M., and Weinberg, M.C. (1997) Radiation effects in glasses used for immobilization of high-level waste and plutonium disposition. Journal of Materials Research, 12, 1946–1978.
Weber, W.J., Ewing, R.C., Catlow, C.R.A., Diaz de la Rubia, T., Hobbs, L.W., Kinoshita, C., Matzke, Hj. Motta, A.T., Nastasi, M., Salje, E.K.H., Vance, E.R., and Zinkle, S.J. (1998) Radiation effects in crystalline ceramics for the immobilization of high-level nuclear waste and plutonium. Journal of Material Research, 13, 1434–1484.
Yokota, Y., Hashimoto, H., and Yamaguchi, T. (1994) Electron beam irradiation of natural zeolites at low and room temperature. Ultramicroscopy, 54, 207–214.
Ziegler, J.F., Biersack, J.P., and Littmark, U. (1985) The stopping and range of ions in solids. Pergamon, New York.
Zinkle, S.J. and Kinoshita, C. (1997) Defect production in ceramics. Journal of Nuclear Materials 251, 200–217.

MANUSCRIPT RECEIVED JANUARY 22, 2002
MANUSCRIPT ACCEPTED SEPTEMBER 19, 2002
MANUSCRIPT HANDLED BY PETER C. BURNS